Eur. Phys. J. B **47**, 47–53 (2005)
DOI: 10.1140/epjb/e2005-00295-y

THE EUROPEAN PHYSICAL JOURNAL B

Conduction mechanism and magnetoresistance in $Gd_{1-x}Pr_xBaCaCu_3O_{7-\delta}$

M. Kariminezhad and M. Akhavan[a]

Magnet Research Laboratory (MRL), Department of Physics, Sharif University of Technology, P.O. Box 11365-9161, Tehran, Iran

Received 11 August 2004 / Received in final form 3 June 2005
Published online 21 September 2005 – © EDP Sciences, Società Italiana di Fisica, Springer-Verlag 2005

Abstract. Tetragonal $Gd_{1-x}Pr_xBaCaCu_3O_{7-\delta}$ ($0 \leq x \leq 1$) polycrystalline samples have been prepared by the standard solid-state reaction, and characterized by XRD and SEM. Rietveld analysis on X-ray diffraction pattern shows site mixing between rare earth (R) and Ca. Contrary to $Gd_{1-x}Pr_xBa_2Cu_3O_{7-\delta}$, a hump on the $\rho(T)$ curve is observed at about 80 K. The normal state resistivity has been analyzed by the two and three dimensional variable range hopping (2&3D-VRH) and Coulomb gap. For low concentration of Pr ($x < 0.5$–0.6, corresponding to the metal-insulator transition), 2D-VRH is the dominant mechanism, but with the increase of x, the 3D-VRH is dominant. Substitution of Ba by Ca highly increases the superconducting granularity. The magnetoresistance measurements have been analyzed by the Ambegaokar and Halperin phase slip model. The field dependences of the pinning energy and critical current density have been studied for different amounts of Pr doping.

PACS. 74.72.Bk Y-based cuprates – 74.25.Ha Magnetic properties – 74.25.Fy Transport properties (electric and thermal conductivity, thermoelectric effects, etc.)

1 Introduction

In the high-T_c superconductor research, essential information has been obtained on the nature of high-T_c superconductivity by the elemental substitution. It has been shown that substitution of the rare earth elements, even magnetic ions, except Pr, on the R site has very little effect on the superconducting properties. For a recent review on this subject see reference [1]. Among all the rare earth ions that form the 123 structure, the only non-superconducting Pr123 has produced a lot of research on compounds of the type $R_{1-x}Pr_xBa_2Cu_3O_{7-\delta}$(RPr123). The Pr substitution has also been studied in other R-based HTSCs families such as $R_{1-x}Pr_xBa_2Cu_4O_8$ (RPr124), $R_{2-x}Pr_xBa_4Cu_7O_{14}$(RPr247), $R_{1-x}Pr_xSr_2Cu_2MO_8$, M = Nb, Ga, V (RPr1212) [2]. Similar to RPr123, full Pr substitution in these systems also resulted in insulating compound. In view of the smaller ionic size difference between Pr and Ba than between Y and Ba, mixing of R and Ba ions will occur still more easily in Pr123. For a recent review on the subject see reference [3]. In contrast, substitution of Sr or Ca on Ba site decreases T_c substantially. These observations imply that Ba site is more important than Y site in superconductivity. A number of structural and compositional investigations, using the oxygen isotope shifted susceptibility [4] and soft X-ray emission spectra [5] have been made to investigate the contribution of the Ba site to the superconductivity of Y123. But, investigation on the properties of the flux dynamics is rare. In the present paper, we investigate the effect of Pr substitution in another family of HTSC, namely the 1113 system, by choosing the $Gd_{1-x}Pr_xBaCaCu_3O_{7-\delta}$ system, and extend our previous work on $Gd_{1-x}Pr_xBaSrCu_3O_{7-\delta}$(GPBSCO) [6]. A comparative study is also made with GdPr123 system.

2 Experimental details

The $Gd_{1-x}Pr_xBaCaCu_3O_{7-\delta}$(GPBCCO) samples with ($0 \leq x \leq 1$) were synthesized by the standard solid-state reaction from Gd_2O_3, Pr_6O_{11}, $BaCO_3$, $SrCO_3$ and CuO powders with the 99.9% purity. The preparation procedures employed are in accordance to reference [7], except that in the present work the grinding was done in an automatic mill. The XRD measurements were done by Philips PW-3710 powder diffractometer with CuK_α radiation ($\lambda = 1.54056$ Å) in the room temperature with 0.02 step width and 0.5 second step time in the range of $0° < 2\theta < 120°$. The XRD results have been analyzed with the DBWS-9807a package based on the Rietveld method. The SEM measurements have been done to determine the size and homogeneity of the samples by JEOL-JXA-840 instrument. The resistance and magnetoresistance of the samples were measured at

[a] e-mail: akhavan@sharif.edu

$J = 0.15$–0.35 A/cm^2 and $f = 40$ Hz by ac four-probe method within the temperature range of 10 to 300 K by a helium closed-cycle refrigerator. A Lake Shore-330 temperature controller with two Pt-100 resistor sensors was used for measuring and controlling the temperature to ± 10 mK. For the magnetoresistivity measurements a magnetic field of maximum 20 kOe was employed.

3 Results and discussion

The powder XRD patterns for GPBCCO shown in Figure 1 indicate that all samples have tetragonal symmetry. Note that the presented intensities are normalized to the main peak in each pattern to 1.0. The observations are consistent with the literature [8]. The XRD patterns of GPBCCO with no Pr content ($x = 0$) consist of some impurity peaks with low intensities. With the increase of Pr content, the intensities of all the impurity peaks decrease. For $x = 1$, the only observed impurity peak is at $2\theta = 43.42$. This observation, consistent with the literature [8], shows that $RBaCaCu_3O_{7-\delta}$ forms better with the light rare earths. In comparison, all GdPr123 samples with $(0 \leq x \leq 1)$ have orthorhombic symmetry, and with increasing Pr content the orthorhombicity decreases. In addition, a small amount of $BaCuO_2$ and $BaPrO_3$ impurity phases are observed in some Pr-rich samples [7]. The presence of $BaCuO_2$ phase is the result of substitution of Pr at Ba site. The absence of $BaCuO_2$ phase in GPBCCO may be the indication of mutual mis-substitution of Pr and Ca. It has been reported that in $RBaCaCu_3O_{7-\delta}$ compounds, the Ca, Ba, and R sites are intermixed [8]. This site switching allows these compounds to form only with those R ions, which can interchange their sites with Ba in R123 structure. The site mixing between R and Ca ions in the compound, results to form the tetragonal structure.

Wang and Bauerle [9] have attributed the relatively low observed (001) reflection intensity at $2\theta = 7.6°$ in $GdBaSrCu_3O_{7-\delta}$ to site mixing between the Gd and Sr ions. We observed that the intensity of this peak in GPBCCO is less than in GPBSCO. Therefore, site mixing between R and Ca in GPBCCO is more than between R and Sr in GPBSCO. Results of our Rietveld refinement support this idea.

The lattice parameters for GPBCCO are obtained from the Rietveld refinement. For GBCCO, GPBCCO ($x = 0.4$), and PBCCO samples, the (a, c) lattice parameters are (3.858 Å, 11.648 Å), (3.862 Å, 11.618 Å) and (3.876 Å, 11.602 Å), respectively. In GPBCCO, the c lattice parameter decreases with the increase of x. Since the ionic radius of Pr^{3+} is larger than Gd^{3+}, we expect an increase in the c lattice parameter with the increase of x. Figure 2 shows a typical measured and calculated XRD intensities for PBCCO sample. In the Rietveld refinement, the impurity peaks were omitted, Lorentzian profile was used, and the background was simulated by a fifth-order polynomial. The temperature factor (B) of the O, Gd, Pr, Ba, Sr, Ca, Cu1, and Cu2 ions was fixed to 1.5, 1, 1, 1.7, 0.8, 0.8, 1.41, 1.5, respectively. The refinement was assisted by constraining the oxygen site occupancies to provide a unit cell oxygen content of 7. Position of atoms in c direction (Z), site occupation factors (N), pattern R-factor (Rp), and weighted pattern R-factor (Rwp) obtained from Rietveld refinement are listed in Table 1 for some of the samples. The results for GBCCO reveal that 64% of Ca atoms occupy the usual Gd site, and for GBSCO, 20% of Sr ions enter the Gd site. All reports on site mixing between Ca and R in $RBaCaCu_3O_{7-\delta}$ agree on the point

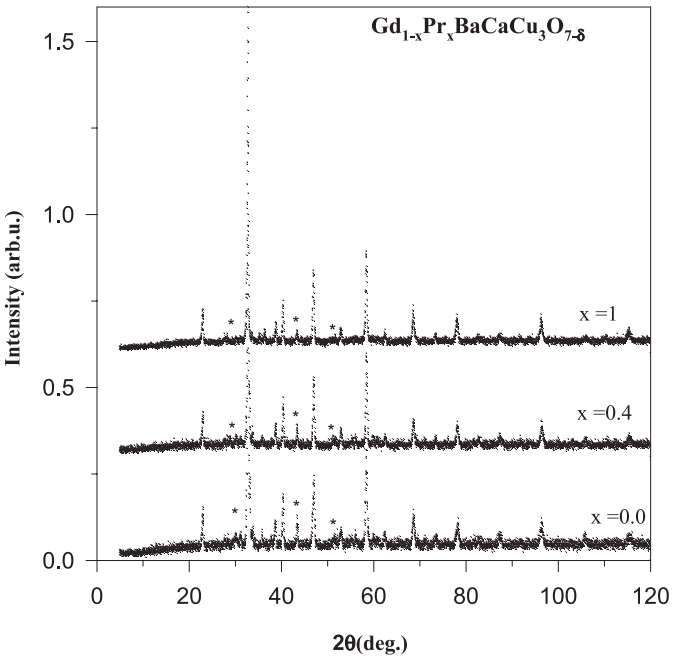

Fig. 1. XRD patterns for GPBCCO with $x = 0.0$, 0.4. 1.0. The (*) signs are the impurity phases.

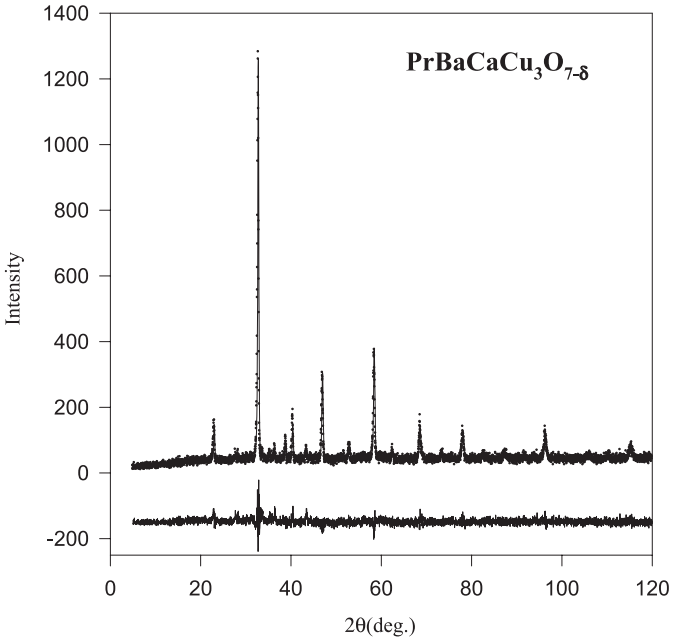

Fig. 2. Calculated (line) and observed (dots) XRD patterns for PBCCO sample. The difference is presented on the bottom.

Table 1. Results of the Rietveld refinement.

Space group position			$Gd_{1-x}Pr_xBaCaCu_3O_{7-\delta}$			$GdBaSrCu_3O_{7-\delta}$
			$x=1$	$x=0.4$	$x=0.0$	
Gd	1d	N	0	0.30652	0.35584	0.71582
		Z	0.5	0.5	0.5	0.5
Pr	1d	N	0.36657	0.03807	0	---
		Z	0.5	0.5	0.5	---
Gd at Ba	2h	N	0	2*0.14674	2*0.32208	2*0.14029
		Z	0.17185	0.17318	0.1756	0.1827
Pr at Ba	2h	N	2*0.31673	2*0.18095	0	---
		Z	0.17185	0.17318	0.1756	---
Ba	2h	N	2*0.5	2*0.5	2*0.5	2*0.5
		Z	0.17185	0.17318	0.1756	0.1827
Ca	2h	N	2*0.18327	2*0.17231	2*0.17792	---
		Z	0.17185	0.17318	0.1756	---
Sr	2h	N	---	---	---	2*0.39815
		Z	---	---	---	0.1827
Ca at R	1d	N	0.63343	0.65541	0.64416	---
		Z	0.5	0.5	0.5	---
Sr at R	1d	N	---	---	---	0.2037
		Z	---	---	---	0.5
Cu2	2g	Z	0.35678	0.36357	0.36398	0.34736
O2	4i	Z	0.38909	0.39326	0.38537	0.37225
O4	2g	Z	0.15535	0.16514	0.16097	0.14306
R_P	---	---	12.37	14.35	13.35	10.23
R_{WP}	---	---	15.82	18.61	17.22	14.2

that Ca occupies the R site. Awana et al. [10], based on the analysis of neutron diffraction data, reveals that nearly 46% of Ca occupies the usual La site.

Figure 3 shows the resistivity versus temperature for GPBCCO samples. With the increase of Pr content x, T_c decreases and the width of transition temperature (ΔT_c) increases. With the increase of the number of insulating parts in the grains, the homogeneity of the grains decreases which leads to larger ΔT_c. With the increase of x, the normal state resistivity increases. In the range $0.0 \leq x \leq 0.5$, $d\rho/dT > 0$, and for $x \geq 0.6$, $d\rho/dT < 0$, leading to occurrence of metal-insulator transition at x_c^{MIT} with $0.5 < x_c^{MIT} < 0.6$, and there is a superconductor-insulator transition at $x_c^{SIT}, 0.5 < x_c^{SIT} < 0.6$. For the GPBSCO samples, $0.5 < x_c^{MIT} < 0.6$ and $0.6 < x_c^{SIT} < 0.7$ [6]. In comparison, for the GdPr123 system, the $x_c^{SIT} = 0.45$ and $x_c^{MIT} = 0.25$ have been reported [7]. The larger values of x_c^{SIT} and x_c^{MIT} in GdPr1113 compared to GdPr123 indicate the lower effect of Pr in suppressing the superconductivity, and hence restitution of superconductivity by Sr substitution for Ba in GdPr123.

For a fixed x, T_c for GPBCCO is smaller and ΔT_c is larger than their corresponding values for GPBSCO [6]: The T_c and ΔT_c for GBSCO are 72 K and 10 K, and for GBCCO are 65 K and 25 K, respectively. This may indicate that inhomogeneity in GPBCCO is considerably more than in GPBSCO. Lower T_c and larger ΔT_c are also observed in $NdBaCaCu_3O_{7-\delta}$ compared to $NdBaSrCu_3O_{7-\delta}$ [11]. In addition, in comparison with Gd123 ($T_c = 92$ K and $\Delta T_c = 1$ K), the site mixing between Sr and Gd could be another factor for the lower T_c and large ΔT_c in GBSCO. As was indicated above for GBCCO sample, the site mixing between Ca and Gd is more than between Sr and Gd in GBSCO, resulting in smaller T_c and larger ΔT_c in GBCCO.

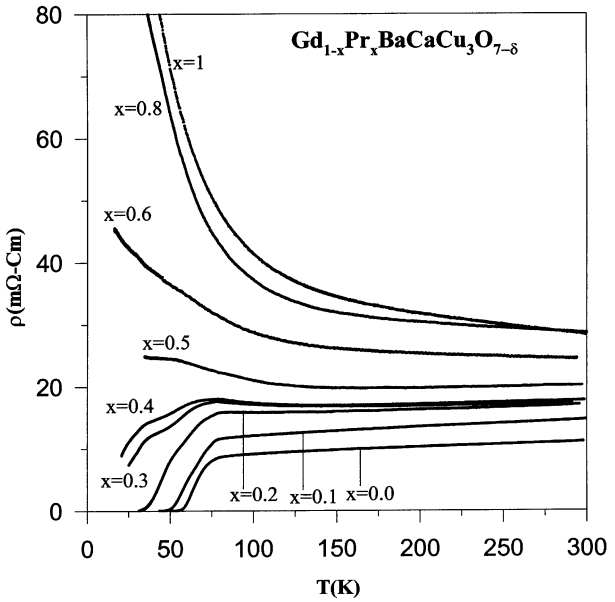

Fig. 3. Resistivity for GPBCCO ($0 \leq x \leq 1$) samples vs. temperature.

An unusual hump on the $\rho(T)$ curve has been observed at about T_p = 75–85 K in GPBCCO samples. Similar hump was observed for GPBSCO samples [6]. For small x, however, no hump appears, and $T_c^{\rm onset}$ remains constant at about 80 K, indicating that the hump exist even for $x = 0.1$ in GPBCCO and GPBSCO samples, but with the increase of x, the hump becomes clearer. Even, for the $x = 0.7$ sample in GPBSCO series, which is an insulator, the hump persists at about 80 K. This may also exist in samples with $x > 0.7$, but because of their large resistivity, it cannot be detected. In GPBCCO, the transition at 80 K is more broadened than in GPBSCO, and becomes clearer for small x compared to GPBSCO series. We do not see this hump in GPBCCO with $x > 0.4$.

Regarding the above hump, it should be noted that they are reproducible through different measurements, and are not due to any measurement errors. Further, the samples with x = 0.4, 0.5, 0.6, and 0.7 of GPBSCO series have been synthesized with different time-temperature calcination and sintering in different batches, and in all cases, the hump persists at about 80 K [12]. Of course, in the samples prepared at higher temperatures, the intensity of the hump is lowered. In addition, $\rho(T)$ were measured with different values of currents and application of magnetic fields. These factors caused no change on the hump. The impurity phases, having non-superconducting nature, cannot be the cause of the hump either. Similar peaks on $\rho(T)$ curves of YPr123[13], YPr1113[14], and $GdBa_{2-x}Pr_x123$ (GdBaPr123) compounds [15] have also been observed. It is noteworthy that in these reports the humps are at about 80 K, same as in our samples, but, in our samples the hump is larger and clearer. It must be noticed that in GPBCCO, the mis-substitution occurs more than in GPBSCO, and the hump becomes clearer at lower x compared to GPBSCO samples.

In the Zou's superconducting Pr123 samples [16], one possibility for the larger c lattice parameter with respect to other 123 structures, is related to the mis-substitution of Ba atoms at Pr site (Ba@Pr). Narozhnyi et al. [17], based on the effective magnetic moment of Pr atom, have concluded that in the Zou's superconducting Pr123 sample there should be some Ba@Pr. We think that Ba@Pr could lead to superconductivity in some parts of the grains at about 80 K, which appears as a hump on the $\rho(T)$ curve [3]. An evidence is that the temperature at which the hump appears on the $\rho(T)$ curve in our samples at about 80 K, has the same value as the superconducting transition temperature of Pr123 in reference [16]. The $T_c^{\rm onset}$ of the Gd1113 sample is 80 K, so the hump may think to be related to some Gd1113 regions, but we do not think so, because with the increase of Pr and decreasing Gd, the hump becomes clearer. These facts can be identified with the increase of Pr: Ba@Pr increases, and hence the hump becomes clearer.

In order to investigate the normal state resistivity, we have fitted 2D-VRH, 3D-VRH, and CG regimes separately for all the samples. In this model, the temperature dependence of resistivity is $\rho(T) = \rho_0(T/T_0)^{2p} \exp(T_0/T)^p$, where p is related to the dimensionality of the hopping process. The T_0 and hopping range (R) for 2D and 3D are defined as: ${T_0}^{\rm 2D} = 14/k_{\rm B}N_{\rm 2D}(E_{\rm F})d^2$, ${T_0}^{\rm 3D} = 21/k_{\rm B}N_{\rm 3D}(E_{\rm F})d^3$, $R_{\rm 2D} = [d/\{\pi N(E_{\rm F})k_BT\}]^{1/3}$, $R_{\rm 3D} = [3d/\{2\pi N(E_{\rm F})k_{\rm B}T\}]^{1/4}$. For definition of the parameters see reference [18]. T_0 and ρ_0, derived from fitting the resistivity data in the temperature range with semilog plot of $\rho(T)$ vs. T^{-p}, is linear. The hump on the $\rho(T)$ curve is not considered in the fitting. The fitting results and the quality of the fit χ^2 are shown in Table 2. For GPBCCO from $x = 0$ to $x = 1$, distinction between 2D-VRH and 3D-VRH is difficult, but preferably, for $x < 0.5$ ($=x_c^{\rm MIT}$), the 2D-VRH and for $x \geq 0.5$, the 3D-VRH is the dominant mechanism. For different amounts of Pr doping, VRH gives very good agreement with the experimental data.

The derived localization length (d) and hopping range (R) for different amount of Pr doping are shown in Figure 4. The localization length is very large for $x = 0$ sample. This means that due to the very large d with respect to the distance of the neighboring atoms, the overlap of the carriers' wave functions is enough for the conduction to perform easily. Therefore, this sample has lower resistivity compared to the sample with $x > 0$. The resistivity of the normal state increases with the increase of x. With the increase of Pr doping, T_0 and the activation energy increase, hence, the conductivity decreases. With the increase of x, d and R decrease. Therefore, Pr doping localizes the carriers in the normal state.

The variations of R and d with x for $x \leq 0.5$ ($=x_c^{\rm MIT}$ in both series) in both series are almost the same. The corresponding data for GPBSCO samples are given by reference [6]. For $x > 0.5$, the variation in GPBSCO is more than in GPBCCO. Similar variation is observed in ρ_{290} versus x in both series. For $x < 0.6$, d in GPBCCO is lower than d in GPBSCO. For $x = 0.6$, d is the same in both series, but for $x > 0.6$, d in GPBCCO is larger than

Table 2. Parameters obtained from VRH fitting for GPBCCO.

	p=1/4			*p=1/3*			*p=1/2*		
x	T_0	ρ_0	χ^2	T_0	ρ_0	χ^2	T_0	ρ_0	χ^2
0.0	568.99	4.73	0.9996	660.44	5.13	0.9998	569.75	5.38	0.9989
0.1	541.81	6.17	0.9995	647.24	6.73	0.9996	567.85	7.07	0.9987
0.2	1551.43	8.55	0.9996	1037.02	8.62	0.9997	630.76	8.59	0.9980
0.3	2388.81	9.11	0.9997	1306.43	9.09	0.9998	692.67	9.01	0.9981
0.4	2138.14	9.22	0.9993	1215.14	9.20	0.9999	660.94	9.09	0.9980
0.5	3389.03	10.85	0.9994	1599.03	10.82	0.9990	763.30	10.70	0.9969
0.6	6897.67	13.14	0.9997	2407.29	13.36	0.9995	917.87	13.42	0.9977
0.8	10 104.41	14.99	0.9997	3089.49	15.53	0.9995	1063.45	15.85	0.9981
1.0	19 364.79	13.51	0.9996	4515.85	14.90	0.9992	1248.81	15.96	0.9974

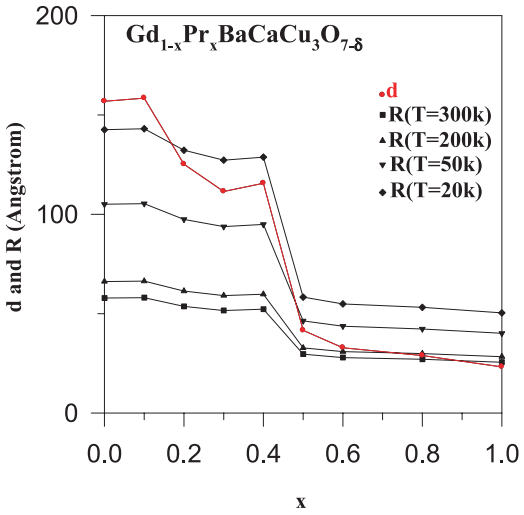

Fig. 4. Localization length and hopping range for GPBCCO samples. The lines are guides to the eye.

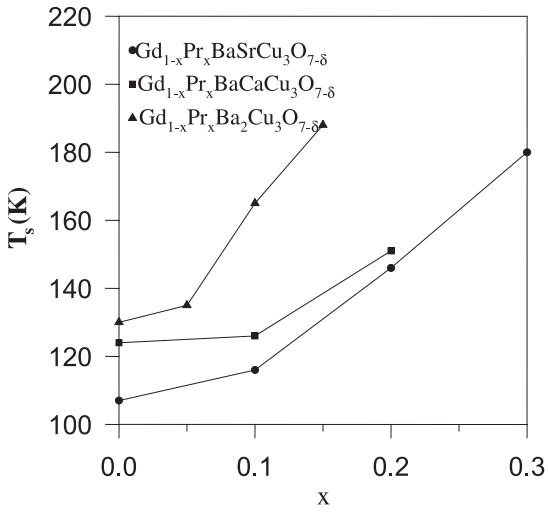

Fig. 5. T_s vs. Pr doping for GPBCCO and GPBSCO samples and data of GdPr123 (after M.R. Mohammadizadeh and Akhavan [19]). The lines are guides to the eye.

in GPBSCO. Similar variation is observed for ρ_{290} versus x in both series. In both series of samples for $x = 0.6$, the values of d and R are 32 Å and 27 Å, respectively. For small x, R is smaller than d. But, for the VRH mechanism, R should be larger than d, e.g., at 50 K for GPBCCO, VRH occurs only for $x \geq 0.5$. With the increase of temperature, due to thermal fluctuations, R decreases. Therefore, the value of x for which the VRH is valid, tends to larger values.

In the samples with $x < x_c{}^{\mathrm{MIT}}$, resistivity vs. temperature deviates from linear behavior at temperature T_s, due to opening of the pseudogap. Figure 5 shows T_s versus Pr doping for GdPr1113 samples and the data of GdPr123 from reference [19]. With increasing x, T_s increases. Variation of T_s versus x in GdPr1113 is more gradual than in GdPr123; for a fixed x, T_s for GdPr1113 is smaller than in GdPr123. The effect of Pr substitution at R site in the 123 structure of HTSC is to increase the pseudogap temperature T_s, although, the Pr substitution in GdPr1113 has a weaker effect on the increase of T_s and suppression of superconductivity.

On the magnetoresistance, $\rho(H)$ curve of the samples, the superconducting transition region is broadened by application of magnetic field. The resistive transition shows two distinct parts: (1) steep part near

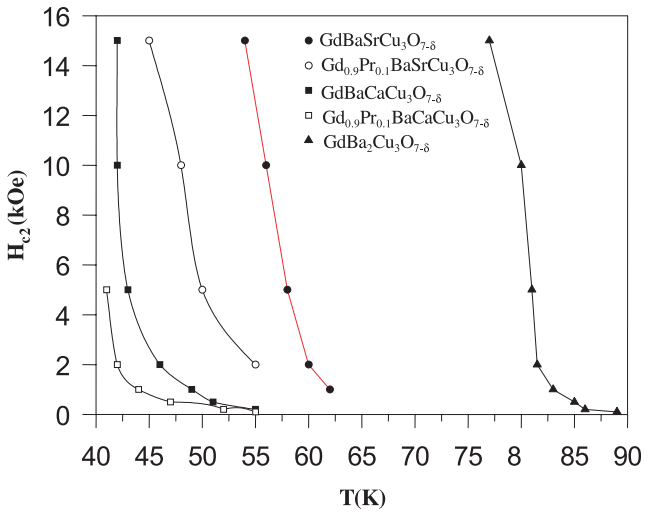

Fig. 6. Intergrain upper critical field (H_{c2}) vs. temperature for $x = 0$ and 0.1 of GPBSCO and GPBCCO samples, and data of Gd123 (after M.R. Mohammadizadeh and M. Akhavan [20]). The lines are guides to the eye.

the onset of superconductivity, where the onset transition temperature remains unchanged. (2) transition tail part. The GPBCCO under magnetic field broadens more than GPBSCO. For fixed x and H, the value of ΔT_H ($\Delta T_H = T_c^{\rho=0}(H) - T_c^{\rho=0}(H=0)$) for GPBCCO is larger than for GPBSCO. The larger ΔT_H correspond to smaller pinning energy in the system. The values of ΔT_H are presented in Table 3. The difference between ΔT_H for the two series of samples increases with the increase of H and Pr doping. In both series of samples, ΔT_H increase with the increase of H and Pr doping. We conclude that the pinning energy in GPBCCO is lower than in GPBSCO. Therefore, GPBCCO have lower critical current and critical field compared to the GPBSCO. From the I–V measurements, we have obtained the same result.

Granular HTSCs, in general, display a two-stage resistive transition $\rho(T)$; and correspondingly, $\mathrm{d}\rho/\mathrm{d}T$ displays a peak and a hump or shoulder in the lower temperature side. The peak, which approximately coincides with the pairing critical temperature T_c, marks the superconducting transition within the grains, and the shoulder is related to the grain coupling. Under lower applied fields, the shoulder readily extends to lower temperatures, while the position and shape of the main peak remains practically unchanged. The temperature, at which the shoulder occurs, T_H, tends to lower temperatures with the increase of magnetic field. From T_H, we can find the intergrain upper critical field (H_{c2}). Figure 6 shows the intergrain H_{c2} vs. temperature for $x = 0$ and 0.1 of GPBCCO and GPBSCO samples, and the data of Gd123 from reference [20]. In fact, these curves show the required magnetic field for suppressing the weak links between the grains. For fixed T, GBCCO has lower H_{c2} than GBSCO. The general trend is the same for GBCCO, GBSCO and Gd123. In GBCCO and GBSCO, there are shifts to lower temperatures, and for GBCCO, there is a larger shift with respect to GBSCO.

Table 3. Values of ΔT_H for GPBSCO and GPBCCO.

$Gd_{1-x}Pr_xBaCaCu_3O_{7-\delta}$		$Gd_{1-x}Pr_xBaSrCu_3O_{7-\delta}$		
$x = 0.1$	$x = 0$	$x = 0.1$	$x = 0$	H(kOe)
8	6	2	1	0.1
>12	10	4	2	0.2
>20	19	7	6	0.5

The decrease in the slope of $H_{c2}(T)$ of GBCCO may be related to the increase of granularity in the sample. Substitution of Ba by Sr or Ca, causes a strong increase of the superconducting granularity and a shift of zero resistivity and of the whole grain coupling phenomenology to lower temperatures without any more fundamental changes in the general trend.

The dissipation part of $\rho(T)$ under magnetic field has been studied by the Ambegaokar and Halperin (AH) theory [21] as $\rho(T) = \rho_n[I_0(\gamma/2)]^{-2}$, where $\gamma = U_0/k_BT = A/H\,(1-t)^q$ in the $I \ll I_c(T)$ limit. For similar procedure in $Gd_{1-x-y}Pr_xCa_yBa_2Cu_3O_{7-\delta}$, see reference [22]. In this fitting process, we use ρ_n, $C(H) = A/H$, and q as free parameters. Critical current density at zero temperature $J_{cj}(0)$ is obtained from the AH theory. The value of $J_{cj}(0)$ for GBCCO, varies from 9×10^3 A/cm^2 at $H = 0.1$ kOe to 2.1×10^3 A/cm^2 at $H = 15$ kOe; the value of $J_{cj}(0)$ for GBSCO, varies from 4×10^4 A/cm^2 at $H = 0.1$ kOe to 2.3×10^3 A/cm^2 at $H = 15$ kOe. At a fixed x and magnetic field, $J_{cj}(0)$ for GPBCCO is less than for GPBSCO. For all samples, the pinning energy and critical current density decrease with the increase of magnetic field. Also, with the increase of Pr doping, $J_{cj}(0)$ decreases to 2.2×10^3 A/cm^2 for $x = 0.2$ of GPBCCO series, and to 6.3×10^3 A/cm^2 for $x = 0.3$ of GPBSCO series at $H = 0.1$ kOe. Figure 7 shows the values of the pinning energy dependent C vs. H for different x for the GPBCCO sample. The figure on the log–log scale shows the two-step variation of C vs. H. The magnetic field dependence of pinning energy for $H \leq 2$ kOe varies in the form $H^{-\alpha}$ and for $H > 2$ kOe, as $H^{-\beta}$. The corresponding behavior for GPBSCO is similar to GPBCCO. The values of α and β for both series are listed in Table 4. With the increase of Pr doping, the values of α and β become closer to each other. In low fields and low level of Pr doping, the average value of α in GdPr123 is 0.2, and in GBSCO and GBCCO is 0.8 and 0.4, respectively. Therefore, pinning energy in GdPr1113 compound is more sensitive to the magnetic field.

4 Conclusions

From a comparative study of $Gd_{1-x}Pr_xBaSrCu_3O_{7\delta}$, $Gd_{1-x}Pr_xBaCaCu_3O_{7\delta}$ (GdPr1113), and $Gd_{1-x}Pr_xBa_2Cu_3O_{7\delta}$ (GdPr123), we conclude that site mixing between R and Ca in GPBCCO is more than between R and Sr in GPBSCO. This site mixing may be the cause of tetragonal structure, low T_c, and large ΔT_c in GdPr1113. Pr substitution in GdPr1113 has a weaker effect on the increase

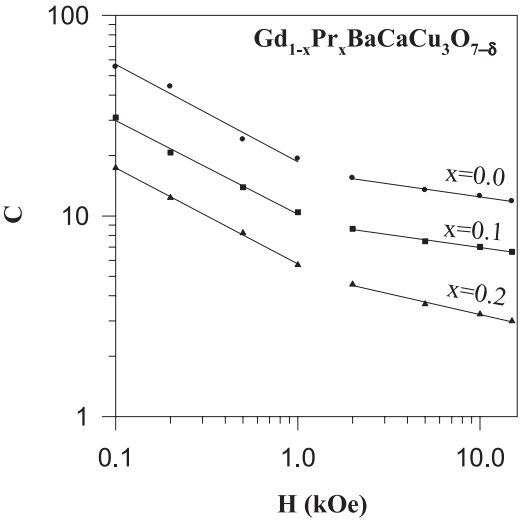

Fig. 7. The log of parameter C vs. logH for GPBCCO with linear fits.

Table 4. Magnetic field dependence power-factors α and β of pinning energy for GPBCCO and GPBSCO.

	$Gd_{1-x}Pr_xBaSrCu_3O_{7-\delta}$		$Gd_{1-x}Pr_xBaCaCu_3O_{7-\delta}$	
x	α	β	α	β
0	0.865	0.099	0.448	0.116
0.1	0.804	0.124	0.427	0.109
0.2	0.751	0.24	0.454	0.178
0.3	0.485	0.253	---	---
0.4	0.25	0.25	---	---

of pseudogap temperature and suppression of superconductivity than GdPr123. Substitution of Ba by Sr or Ca, causes strong increase of the superconducting granularity and shift of zero resistivity and of the whole grain coupling phenomenology to lower temperatures without any more fundamental changes in the general trend.

The authors wish to thank M. Mirzadeh, P. Maleki, Z. Mokhtari, and H. Khosroabadi for technical assistance and fruitful discussions. This work was supported in part by the Offices of the Vice President for Research and the Dean of Graduate Studies at Sharif University of Technology.

References

1. M. Akhavan, Phys. B **321**, 265 (2002)
2. V.P.S Awana, J. Horvat, S.X. Dou, A. Sedky, A.V. Narlikar, J. Magn. Magn. Mater. **182**, L280 (1998)
3. M. Akhavan, Phys. Stat. Sol. (b) **241**, 1242 (2004)
4. G. Zhao, A.P.B. Zinha, D.E. Morris, Phys. C **297**, 23 (1998)
5. D.R. Mueller, J.S. Wallace, J.J. Jia, W.L. O'Brien, Q.Y. Dong, T.A. Callcott, K.E. Miyano, D.L. Ederer, Phys. Rev. B **52**, 9702 (1995)
6. M. Kariminezhad, H. Khosroabadi, M. Akhavan, Phys. Stat. Sol. (c) **1**, 1855 (2004)
7. Z. Yamani, M. Akhavan, Solid State Commun. **107**, 197 (1998)
8. V.P.S. Awana, C.A. Cardoso, O.F. de Lima, R. Singh, A.V. Narlikar, W.B. Yelon, S.K. Malik, Phys. C **316**, 113 (1999)
9. X.Z. Wang, D. Bäuerle, Phys. C **176**, 507 (1991)
10. V.P.S. Awana, S.X. Dou, S.K. Malik, R. Singh, A.V. Narlikar, D.A. Landinez Tellez, J.M. Ferreira, J. Albino Aguiar, S. Uma, E. Gmelin, W.B. Yelon, J. Magn. Magn. Mater. **187**, 192 (1998)
11. R. Ganguly, I.K. Gopalakrishnan, J.V. Yakhmi, Phys. C **256**, 51 (1996)
12. M. Kariminezhad, M. Akhavan, submitted for publication by J. Supercond. (2005)
13. J.L. Peng, P. Klavins, R.N. Shelton, H.B. Radousky, P.A. Hahn, L. Bernardez, Phys. Rev. B **40**, 4517 (1989)
14. G. Cao, Y. Qian, Z. Chen, X. Li, H. Wu, Y. Zhang, Phys. Lett. A **196**, 263 (1994)
15. M.R. Mohammadizadeh, M. Akhavan, Phys. Rev. B **68**, 104516 (2003)
16. Z. Zou, J. Ye, K. Oka, Y. Nishihara, Phys. Rev. Lett. **80**, 1074 (1998)
17. V.N. Narozhnyi, S.-L. Drechsler, Phys. Rev. Lett. **82,** 461 (1999)
18. M.R. Mohammadizadeh, M. Akhavan, Eur. Phys. J. B **33**, 381 (2003)
19. M.R. Mohammadizadeh, M. Akhavan, Phys. B **336**, 410 (2003)
20. M.R. Mohammadizadeh, M. Akhavan, Supercond. Sci. Technol. **16**, 1216 (2003)
21. V. Ambegaokar, B.I. Halperin, Phys. Rev. Lett. **22**, 1364 (1969)
22. H. Shakeripour, M. Akhavan Supercond. Sci. Technol. **14**, 234 (2001)